ADVANCED ELECTRONIC MATERIALS
www.advelectronicmat.de

Check for updates

Resonant Tunneling and Negative Differential Resistance in Black Phosphorus Vertical Heterostructures

*Kai Xu, Eric Wynne, and Wenjuan Zhu**

Resonant tunneling diodes with negative differential resistance (NDR) have attracted significant attention due to their unique quantum resonant tunneling phenomena and potential applications in terahertz emission/detection and high-density logic/memory. In this paper, resonant tunneling devices, where the carriers tunnel through a hexagonal boron nitride (hBN) barrier sandwiched by two black phosphorus (BP) layers, are explored. The resonance occurs when the energy bands of the two black phosphorus layers are aligned. The conductive atomic force microscopy (CAFM) measurements reveal prominent NDR peaks with large peak-to-valley ratios at room temperature. It is found that the positions of the NDR peaks are very sensitive to the amplitude and the shape of the voltage waveform used in CAFM, which can be explained by the charge trapping effect. Furthermore, resonant tunneling transistors are demonstrated based on BP/hBN/BP stacks in which the locations of the NDR peaks are tunable by the electrostatic gating. As compared to the traditional tunneling diodes based on bulk materials, the tunneling devices based on thin boron nitride tunneling barrier and high mobility black phosphorus offer ultra-high-speed response. This feature, together with the NDR characteristics, provides the potential for applications in THz oscillators and multi-value logic devices.

A resonant tunneling diode (RTD) is a two-terminal device based on quantum resonant tunneling with the characteristics of fast response and negative differential resistance (NDR).[1–5] These devices can serve as sensitive tools for the measurement of electron tunneling, inter-subband transition, and phonon-assisted tunneling.[5,6] RTDs have broad applications from terahertz oscillators, to multi-value logic, and to resistance switching memories.[7–14] Various material stacks have been used in RTDs, including Si, Ge, SiGe,[15] group III-V,[12,16,17] group II-VI, mixed crystalline, and amorphous materials. Although much research has focused on III-V material systems, the large device-to-device variation in performance limits their widespread application in commercial products. The key factors that deteriorate the performance of III-V based RTDs are lattice mismatch (and associated dislocations), impurity scattering, polarization charges, and instability of space charge.[18] Recently, 2D crystals have been used in RTD devices. A symmetric tunneling field-effect transistor (SymFET) and bilayer pseudo spin field-effect transistor (BiSFET) based on two graphene layers separated by an insulator were proposed theoretically,[19–21] and graphene-based tunnel diodes were demonstrated experimentally with NDR characteristics.[22–24] However, due to zero bandgap and low density of states in graphene, the peak-to-valley ratios (PVRs) in graphene RTDs are very limited (typically less than 4 at room temperature). It is theoretically predicted that RTDs based on transition metal dichalcogenides and black phosphorus can provide sharper resonant current peaks and higher PVRs.[25,26] In this paper, we demonstrate RTD and resonant tunneling transistors based on BP/hBN/BP heterostructures with prominent resonant tunneling. The thin boron nitride layer enables high tunneling current, while the high-mobility black phosphorus facilitates fast response, making these devices very promising for THz applications.

We investigated the NDR effect in the BP/BN/BP heterostructures using CAFM. The device structure is illustrated in **Figure 1**a. The process used to create the heterostructure was an adaptation of the "hot pick-up" technique, in which a piece of polydimethylsiloxane (PDMS) is coated in polypropylene carbonate (PPC) and is then pressed against flakes of material on a silicon substrate.[27] The black phosphorus and boron nitride flakes were picked up from the silicon dioxide substrate and then stacked on a gold-coated silicon wafer piece, as shown in Figure 1a. The thicknesses of the hBN tunneling barrier, the top black phosphorus layer, and the bottom black phosphorus layer are ≈10, ≈55, and ≈150 nm, respectively, measured using atomic force microscopy (AFM).

The resonant tunneling characteristic of a BP/hBN/BP heterostructure on Au/Si substrate was measured using CAFM at room temperature in atmosphere. The CAFM tips have Cr/Pt coating with tip radius of less than 25 nm. The sample bias, V_B, was applied to the substrate. A frequency of 0.1 Hz was used for all voltage waveforms during testing. A typical waveform is illustrated in Figure 1b. The current compliance was set as 20 nA to protect the device. Figure 1c shows the IVs of a BP/hBN/BP heterostructure measured 12 times using the waveforms

Dr. K. Xu, E. Wynne, Prof. W. Zhu
Electrical and Computer Engineering
University of Illinois at Urbana-Champaign
Urbana, Illinois 61801, USA
E-mail: wjzhu@illinois.edu

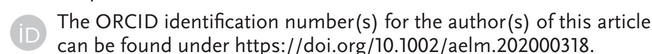
The ORCID identification number(s) for the author(s) of this article can be found under https://doi.org/10.1002/aelm.202000318.

DOI: 10.1002/aelm.202000318

© 2020 WILEY-VCH Verlag GmbH & Co. KGaA, Weinheim

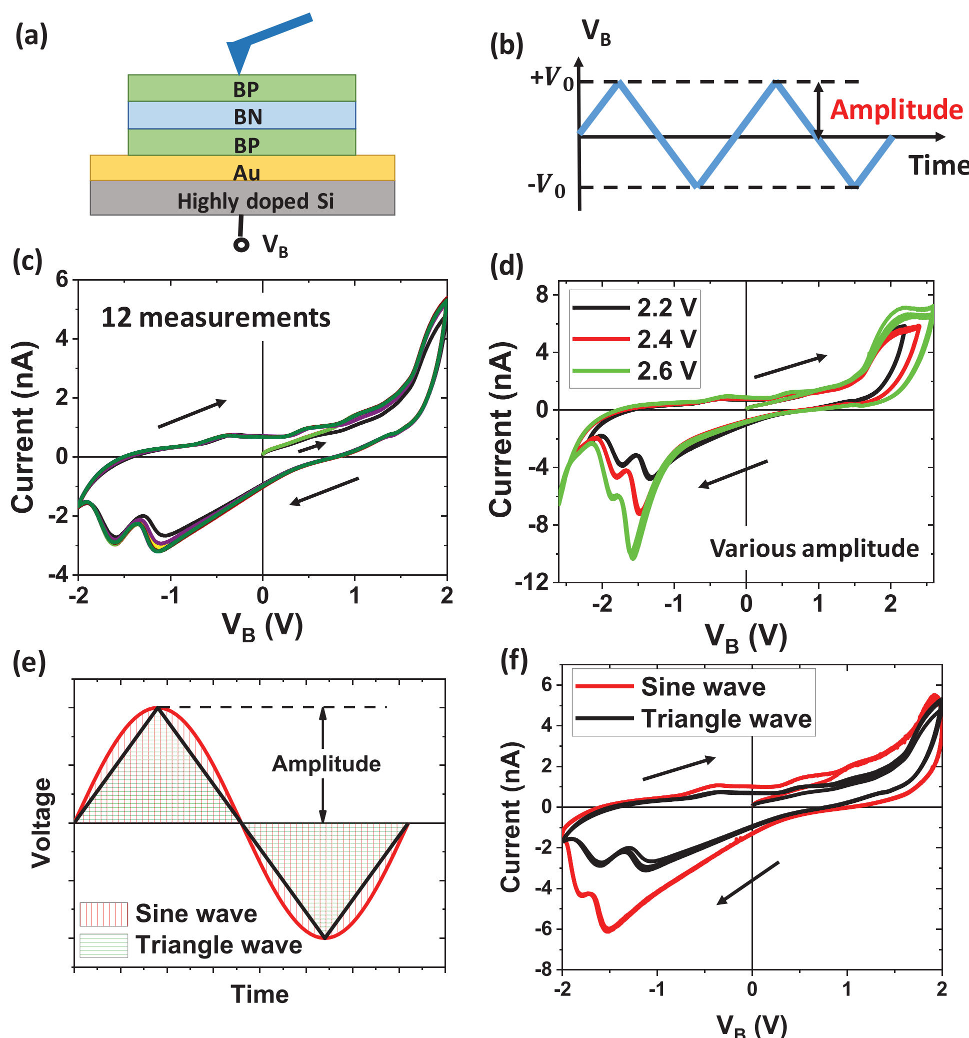

Figure 1. CAFM measurements on RTDs based on BP/hBN/BP heterostructures. a) Illustration of a RTD for CAFM measurement. b) Schematic of a waveform applied to the RTD. c) Overlay of 12 IV curves measured consecutively on a BP/hBN/BP heterostructure using the waveforms with the same amplitude 2 V. d) IV curves of the same BP/hBN/BP heterostructure measured using the waveforms with various amplitudes: 2.2, 2.4, and 2.6 V. For each type of the waveform, four IV measurements were taken. e) Illustration of the triangular and sine waveforms used in the CAFM measurements. f) IV curves of a BP/hBN/BP heterostructure measured using the triangular and sine waveforms, both with an amplitude of 2 V and a frequency of 0.1 Hz.

with the same amplitude 2 V. The most noticeable feature of the data is the presence of pronounced peaks in the current. Beyond the peaks, there are clear negative differential conductance regions. The peak positions are nearly the same for the 12 measurements, indicating that the measurement is repeatable and reliable. Hystereses are clearly observed in these IVs. Then we increase the amplitude of the waveform from 2.2 to 2.6 V, shown in Figure 1d. As the amplitude of the voltage waveform increases, the peaks shift to more negative direction, that is, $|V_p|$ increases. The position of the NDR peak can also be influenced by the shape of the voltage waveform. We compared the tunneling current of the BP/hBN/BP heterostructure measured using a triangular waveform and a sine waveform, as shown in Figure 1e,f. We notice that the peak voltage $|V_p|$ tested with sine waveform is higher than that with triangular waveform.

These phenomena can be explained by the resonant tunneling between the two black phosphorus layers and the band offsets induced by charge trapping. The IV loop of a BP/hBN/BP heterostructure is illustrated in **Figure 2**a and the energy diagrams corresponding to points 1–4 are shown in Figure 2b–e. It is assumed that the doping level in the top and bottom black phosphorus are similar. At equilibrium, the conduction and valence bands of the two black phosphorus layers are roughly aligned, as shown in Figure 2b. When a positive voltage is applied on the bottom black phosphorus ($V_B > 0$), the energy band of the bottom black phosphorus layer is lower than that of the top black phosphorus layer (Figure 2c). For most energy levels, there is a large wavevector mismatch between the two black phosphorus layers. Due to the requirement of energy and momentum conservation, direct tunneling of the carriers from one black phosphorus layer to the other is prohibited. Therefore, resonant tunneling is not observed when the substrate bias is swept from zero to a positive value. Note that when the bottom BP is under positive bias, the conduction/valence bands

 © 2020 WILEY-VCH Verlag GmbH & Co. KGaA, Weinheim

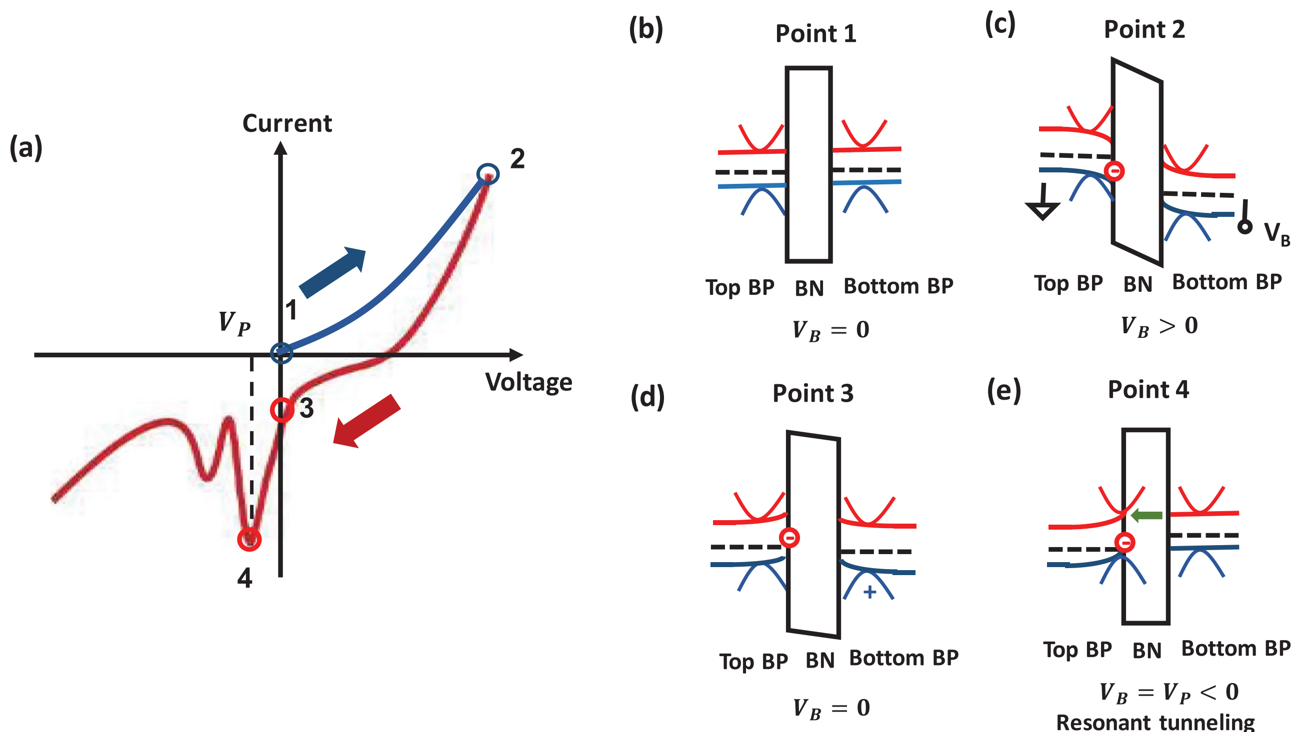

Figure 2. Hypothetical mechanism of the NDR effect in BP/hBN/BP heterostructures observed in CAFM measurements. a) Illustration of the CAFM IV characteristic of a BP/hBN/BP heterostructure when the substrate bias is swept from zero to $+V_0$, then swept from $+V_0$ to $-V_0$. b–e) Energy diagrams of the BP/hBN/BP heterostructure, corresponding to the 1–4 points of the IV curve shown in (a) respectively. b) Point 1: substrate bias is zero ($V_B = 0$), Fermi level is constant and the current equals to zero. c) Point 2: the substrate bias is positive ($V_B > 0$). As the interface states located at the top BP/BN interface move below the Fermi level, they tend to capture more electrons. d) Point 3: the substrate bias is swept back to zero. The remaining trapped charges at the interface induce a small band offset between the top and the bottom BP layers. e) Point 4: the substrate bias is negative ($V_B < 0$). The energy band of the bottom BP layer rises. When the energy bands between the two BP layers are re-aligned, resonant tunneling occurs, which results in a local maximum of the tunneling current.

of the top BP bend downward, that is, more energy levels at the BP/BN interface are below the Fermi level as compared to the case at equilibrium. If there are gap states at the BP/BN interface, more electrons will be trapped in these interface states. When the substrate bias is swept back from the positive to the negative value at high speed, some of the trapped charges may not have enough time to be released by the traps. These trapped charges can lead to a band offset between the two black phosphorus layers (Figure 2d). When a negative bias is applied to the substrate, it can raise the energy band of the bottom black phosphorus layer. When the two energy bands are brought back to alignment (Figure 2e), the energies and momentums of these two black phosphorus layers are matched simultaneously, the carriers tunnel resonantly, and the current reaches a local maximum. As the bias increases further, the two bands will be out of alignment and the current will decrease again, leading to the NDR regime.

As the amplitude of the voltage waveform increases, the charges built up in the heterostructures increase, which results in larger band offsets between two black phosphorus layers. Consequently, larger bias is required to re-align the energy bands of the two black phosphorus layers, that is, the peak voltage $|V_p|$ increases. The dependence of the peak voltage $|V_p|$ on the shape of the waveform can also be explained by this model. Notice that the shaded area of the waveform corresponds to the integration of the voltage over time ($V(t)dt$). For a given amplitude and frequency of the voltage waveform, the shaded area is larger in sine waveform than in triangular waveform. This means that the charges pumped into the heterostructure are greater for the sine waveform than for the triangular waveform, assuming that the current density increases with applied voltage. Therefore the band offset is larger and the absolute value of the peak voltage $|V_p|$ is higher for the sine waveform than for the triangular waveform. Note that there are multiple peaks in the IV curves, which can be explained by the multiple sub-bands in the thick black phosphorus layers. These multiple resonant peaks were also observed in RTDs based on multilayer graphene and III-V materials with multiple sub-bands.[28–30] When any of these sub-bands are aligned, a sharp increase in tunneling current occurs, creating an NDR peak.

It is well known that PVR is a key parameter for RTD. The maximum PVR in our BP/hBN/BP heterostructure is about 4.5. We compare it with the PVRs of the RTDs based on other 2D heterostructures reported recently.[23,24,30] The results are summarized in **Table 1**. The PVR of the BP/hBN/BP heterostructure is larger than that of other structures especially at room temperature, indicating that BP/hBN/BP heterostructure has great potential in tunneling devices.

In order to control the peak voltage electrically, three-terminal resonant tunneling transistors with embedded-gates

© 2020 WILEY-VCH Verlag GmbH & Co. KGaA, Weinheim

Table 1. Comparison of the RVRs in various RTDs based on 2D heterostructures.

Heterostructure	PVR	Temperature	V_G	Refs.
Bilayer Gr/BN/Gr	1.5	10 K	20 V	[23]
Bilayer Gr/BN/Gr	1.8	RT	40 V	[23]
Gr/BN/Gr	4	7 K	−60 V	[24]
Gr/BN/Gr	1.4	RT	50 V	[24]
WSe_2/BN/WSe_2	1.2	RT	−7.4 V, −19 V	[30]
BP/BN/BP	4.5	RT	w/o	Our work

Note: "Gr" stands for "graphene". "RT" stands for "room temperature".

were fabricated. The schematic and the optical image of a resonant tunneling transistor based on BP/hBN/BP heterostructure are shown in **Figure 3**a. The embedded gate was made of 5 nm Ti/20 nm Au, and the bottom gate dielectric is 20 nm HfO_2 grown by atomic layer deposition (ALD). The top and bottom BP thickness are 18 and 19 nm, respectively. The BN thickness is estimated to be 5 nm based on AFM. The interlayer currents were measured as a function of interlayer bias V_{TL}, at various back gate voltages. Resonant tunneling and NDR are observed clearly at 20 K, as shown in Figure 3b.

The observed NDR can be explained by the momentum conserving tunneling. **Figure 4** illustrates the energy band diagrams of the device at various biasing conditions. When the interlayer bias is zero ($V_{TL} = 0$), the tunneling current is zero (Figure 4a). Note that the energy bands of the top and bottom BP layer may have an offset, which is attributed to the difference of the trap charge densities in the HfO_2 layer and the boron nitride layer, the difference of work functions in the embedded gate (Au) and the BP layer, and/or the adsorption of moisture on the top BP layer. Here, we assume that the energy band of the top BP layer is higher than that in the bottom BP layer at equilibrium. When the interlayer bias is small and the two energy bands are misaligned, in order for a carrier to tunnel from one BP layer to the other, its in-plane wavevector k must change. Such a change is forbidden unless the tunneling event is accompanied by a scattering process. The tunneling probability is low in this case. As the interlayer bias increases, the energy band of the top BP layer shifts downward (Figure 4b). When the energy bands of the two BP layers are aligned, carriers can tunnel from one layer to the other layer while conserving momentum and energy simultaneously. The resonant tunneling occurs and the interlayer current reaches a local maximum. When the interlayer bias V_{TL} increases further, the energy bands of the two BP layers are misaligned again, the tunneling is off-resonance and the interlayer current decreases.

The locations of the NDR peaks are tunable by the gate voltage, as shown in inset of Figure 3b. As the back gate voltage increases, the interlayer bias at resonance increases, which can be understood as follows. A positive bottom gate voltage will introduce more n-type doping in the bottom BP (Figure 4c). In order to achieve band alignment between the two BP layers for resonant tunneling, a higher V_{TL} is required to lower the energy band of the top BP layer (Figure 4d).

This work demonstrates the resonant tunneling and NDR effect in BP/hBN/BP vertical heterostructures. Our devices show pronounced NDR peaks with high PVR at room temperature. We found that the NDR peak locations are sensitive to the

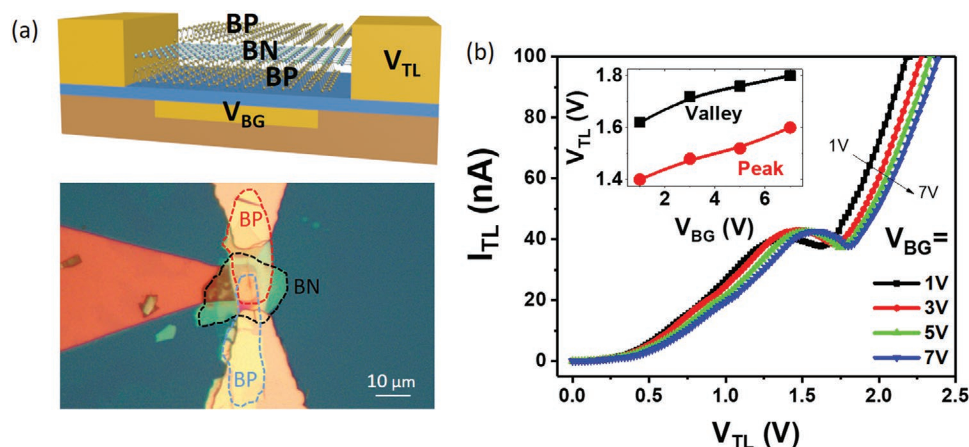

Figure 3. Resonant tunneling transistor based on BP/hBN/BP heterostructure. a) Schematic and optical image of the BP/hBN/BP resonant tunneling transistor. b) Interlayer tunneling current as a function of interlayer bias measured at various back gate bias at 20 K. The inset shows the peak and valley position of the resonant tunneling as a function of back gate bias.

© 2020 WILEY-VCH Verlag GmbH & Co. KGaA, Weinheim

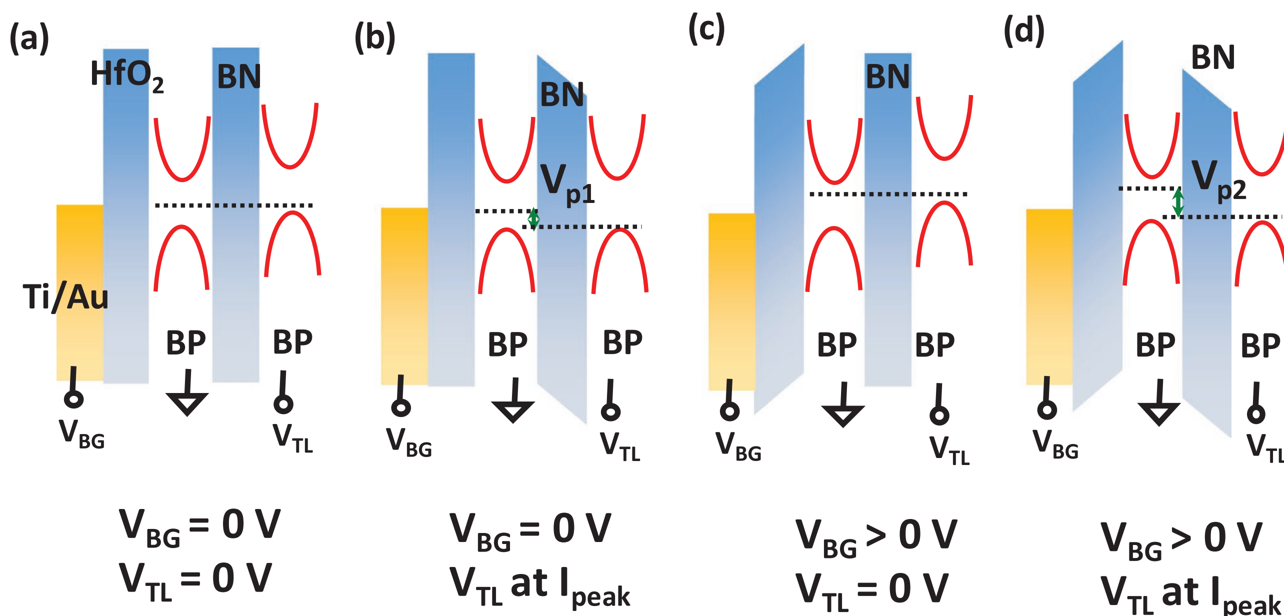

Figure 4. Mechanism of the NDR effect in the resonant tunneling transistors based on BP/hBN/BP heterostructures. The energy band diagrams of the resonant tunneling transistor at various biasing conditions: a) $V_{BG} = 0$ and $V_{TL} = 0$; b) $V_{BG} = 0$ and V_{TL} is at the voltage where the tunneling current reaches a peak; c) $V_{BG} > 0$ and $V_{TL} = 0$; d) $V_{BG} > 0$ and V_{TL} is at the voltage where the tunneling current reaches a peak.

amplitude and the shape of the voltage waveform. Unlike the traditional double-barrier resonant tunneling diodes based on bulk materials, these 2D tunneling diodes have only one tunneling barrier, which can significantly reduce the dwell time in the quantum well and improve the response speed of the device. Furthermore, resonant tunneling transistors based on BP/hBN/BP heterostructures were also demonstrated. The peak voltages can be effectively modulated via electrostatic gating in the resonant tunneling transistors. As compared to graphene-based tunnel diodes, the sizable bandgap of black phosphorus can effectively reduce the valley current and further improve the PVR ratio. These features together with the multiple NDR characteristics will enable a broad range of applications, including terahertz oscillators, memories, logic switches, nano-thermometers, and "neuron-like" circuits.

Acknowledgements

The authors would like to acknowledge the support from National Science Foundation (NSF) under Grants ECCS 16–11279 and ECCS 16–53241 CAR, and from Office of Naval Research (ONR) under grant NAVY N00014-17-1-2973.

Conflict of Interest

The authors declare no conflict of interest.

Author Contributions

K.X. and E.W. contributed equally to this work. The manuscript was written through contributions of all authors. All authors have approved the final version of the manuscript.

Keywords

black phosphorus, boron nitride, heterostructures, negative differential resistance, resonant tunneling diodes

Received: March 28, 2020
Revised: May 23, 2020
Published online: July 15, 2020

[1] H. Mizuta, T. Tanoue, *Cambridge Studies in Semiconductor Physics and Microelectronic Engineering*, 2, [Online] Cambridge University Press: Cambridge, New York **1995**, pp. 1 online resource (xiv, 239 p.).
[2] L. L. Chang, L. Esaki, R. Tsu, *Appl. Phys. Lett.* **1974**, *24*, 593.
[3] W. R. Frensley, *Phys. Rev. Lett.* **1986**, *57*, 2853.
[4] Q. H. Wang, K. Kalantar-Zadeh, A. Kis, J. N. Coleman, M. S. Strano, *Nat. Nanotechnol.* **2012**, *7*, 699.
[5] S. Choi, Z. Shaolin, W. Yang, *J. Korean Phys. Soc.* **2014**, *64*, 1550.
[6] J. P. Sun, G. I. Haddad, P. Mazumder, J. N. Schulman, *P Ieee* **1998**, *86*, 641.
[7] T. Waho, A. Yamada, H. Okuyama, V. Khorenko, T. Do, W. Prost, *Ieee Int Symp Circ S* **2007**, 129.
[8] Y. Klofai, B. Z. Essimbi, D. Jager, *Phys. Scr.* **2015**, *90*, 025002.
[9] A. L. Elgreatly, A. A. Shaaban, E. M. El-RabaieEnhancement of DRAMs Performance Using Resonant Tunneling Diode Buffer, 2014 The 1st International Conference on Information Technology, Computer, and Electrical Engineering, 8-8 Nov. 2014, **2014**; pp 16.
[10] A. Pfenning, F. Hartmann, M. R. S. Dias, L. K. Castelano, C. Sussmeier, F. Langer, S. Hofling, M. Kamp, G. E. Marques, L. Worschech, V. Lopez-Richard, *ACS Nano* **2015**, *9*, 6271.
[11] S. K. Diamond, E. Ozbay, M. J. W. Rodwell, D. M. Bloom, Y. C. Pao, J. S. Harris, *Appl. Phys. Lett.* **1989**, *54*, 153.
[12] G. Keller, A. Tchegho, B. Munstermann, W. Prost, F. J. Tegude, *Conf P Indium Phosph* **2013**, 36.
[13] K.-J. Gan, J.-J. Lu, W.-K. Yeh, Y.-H. Chen, Y.-W. Chen, *Eng. Sci. Technol.* **2016**, *19*, 888.

© 2020 WILEY-VCH Verlag GmbH & Co. KGaA, Weinheim

[14] M. Asada, S. Suzuki, N. Kishimoto, *Jpn. J. Appl. Phys.* **2008**, *47*, 4375.
[15] A. Ramesh, T. A. Growden, P. R. Berger, R. Loo, W. Vandervorst, B. Douhard, M. Caymax, *IEEE Trans. Electron Devices* **2012**, *59*, 602.
[16] E. R. Brown, T. C. L. G. Sollner, C. D. Parker, W. D. Goodhue, C. L. Chen, *Appl. Phys. Lett.* **1989**, *55*, 1777.
[17] T. Maekawa, H. Kanaya, S. Suzuki, M. Asada, *Electron. Lett.* **2014**, *50*, 1214.
[18] M. Hermann, E. Monroy, A. Helman, B. Baur, M. Albrecht, B. Daudin, O. Ambacher, M. Stutzmann, M. Eickhoff, *Physica Status Solidi(c)* **2004**, *1*, 2210.
[19] L. F. Register, X. Mou, D. Reddy, W. Jung, I. Sodeman, D. Pesin, A. Hassibi, A. H. MacDonald, S. K. Banerjee, *ECS Trans.* **2012**, *45*, 3.
[20] P. Zhao, R. M. Feenstra, G. Gu, D. Jena, *IEEE Trans. Electron Devices* **2013**, *60*, 951.
[21] J. Gaskell, L. Eaves, K. S. Novoselov, A. Mishchenko, A. K. Geim, T. M. Fromhold, M. T. Greenaway, *Appl. Phys. Lett.* **2015**, *107*, 103105.
[22] S. Kang, B. Fallahazad, K. Lee, H. Movva, K. Kim, C. M. Corbet, T. Taniguchi, K. Watanabe, L. Colombo, L. F. Register, E. Tutuc, S. K. Banerjee, *IEEE Electron Device Lett.* **2015**, *36*, 405.
[23] B. Fallahazad, K. Lee, S. Kang, J. M. Xue, S. Larentis, C. Corbet, K. Kim, H. C. P. Movva, T. Taniguchi, K. Watanabe, L. F. Register, S. K. Banerjee, E. Tutuc, *Nano Lett.* **2015**, *15*, 428.
[24] L. Britnell, R. V. Gorbachev, A. K. Geim, L. A. Ponomarenko, A. Mishchenko, M. T. Greenaway, T. M. Fromhold, K. S. Novoselov, L. Eaves, *Nat. Commun.* **2013**, *4*.
[25] G. C. Constantinescu, N. D. M. Hine, *Nano Lett.* **2016**, *16*, 2586.
[26] P. M. Campbell, A. Tarasov, C. A. Joiner, W. J. Ready, E. M. Vogel, *ACS Nano* **2015**, *9*, 5000.
[27] F. Pizzocchero, L. Gammelgaard, B. S. Jessen, J. M. Caridad, L. Wang, J. Hone, P. Boggild, T. J. Booth, *Nat. Commun.* **2016**, *7*, 11894.
[28] S. Kang, N. Prasad, H. C. P. Movva, A. Rai, K. Kim, X. H. Mou, T. Taniguchi, K. Watanabe, L. F. Register, E. Tutuc, S. K. Banerjee, *Nano Lett.* **2016**, *16*, 4975.
[29] P. M. Campbell, A. Tarasov, C. A. Joiner, W. J. Ready, E. M. Vogel, *J. Appl. Phys.* **2016**, *119*, 024503.
[30] K. Kim, N. Prasad, H. C. P. Movva, G. W. Burg, Y. M. Wang, S. Larentis, T. Taniguchi, K. Watanabe, L. F. Register, E. Tutuc, *Nano Lett.* **2018**, *18*, 5967.

© 2020 WILEY-VCH Verlag GmbH & Co. KGaA, Weinheim